Karlsruhe Institute of Technology

Damage and Young's modulus reduction in silica by hydroxyl generation

T. Fett, G. Schell

KIT SCIENTIFIC WORKING PAPERS 106

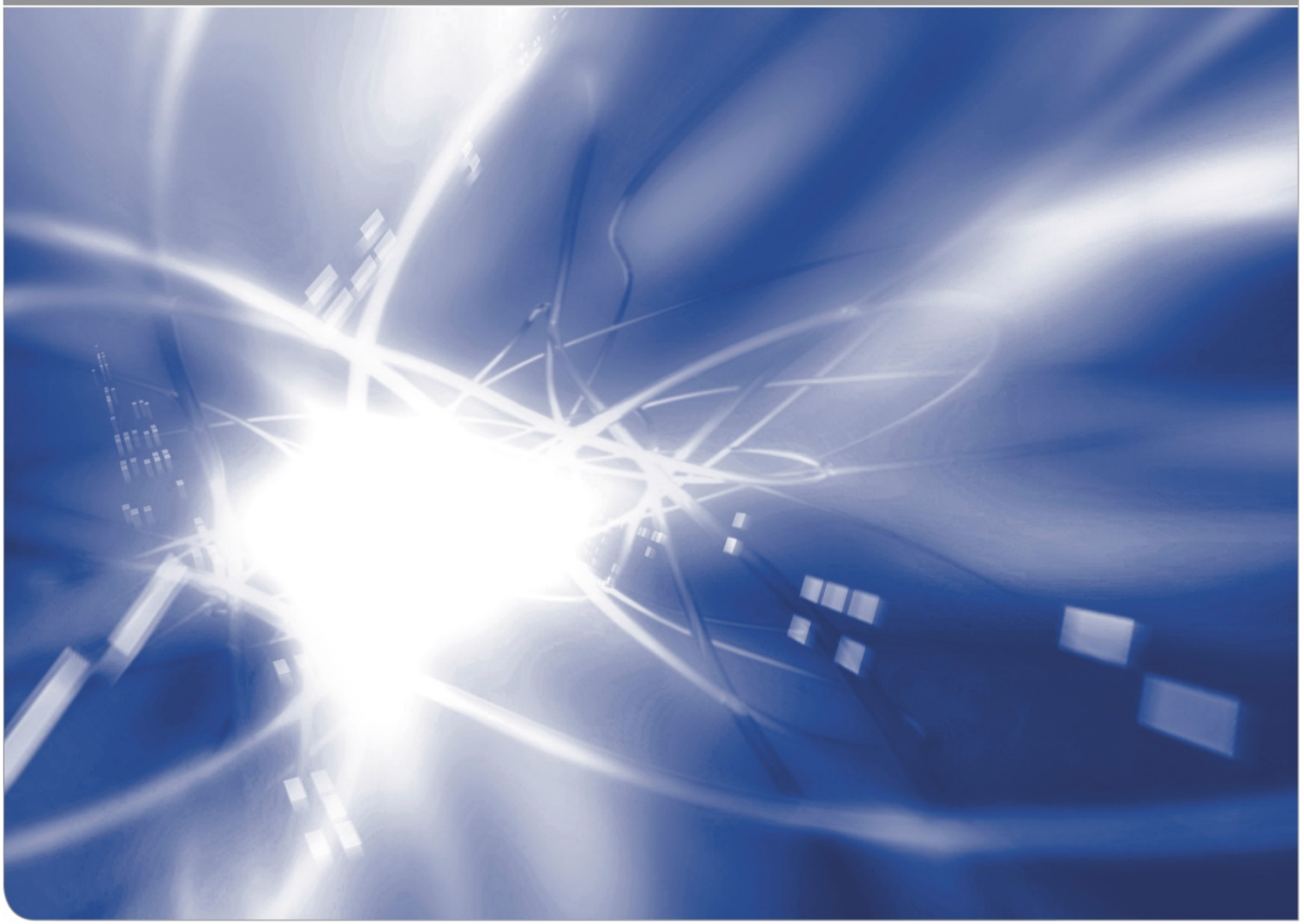

IAM Institute for Applied Materials

Impressum

Karlsruher Institut für Technologie (KIT)
www.kit.edu

2019

ISSN: 2194-1629

Abstract

Water diffusion into silica glass results in a thin zone near the surface of the glass. In this zone the water reacts with the SiO_2 structure and "damages" the originally intact SiO_2 rings. The consequence is a reduced Young's module. This effect can be described by use of continuum damage mechanics according to Kachanov [1] and Lemaitre [2].

In this paper the dependency between hydroxyl concentration and damage will be described for large water concentrations by using the pore models of Wang [3] and Phani and Niogy [4]. As an application, the hydroxyl concentration at crack tips is computed and crack-tip stress intensity factor is estimated.

Contents

1 Damage by hydroxyl generation

When water comes in contact with silica [SiO_2], it reacts with the silica network according to

$$\equiv\text{Si-O-Si}\equiv + H_2O \leftrightarrow \equiv\text{SiOH+HOSi}\equiv \tag{1}$$

and generates hydroxyl $S = [\equiv\text{SiOH}]$. In (1) $[H_2O]=C$ is the concentration of the molecular water.

When a hydroxyl has been formed, the initial silica ring is broken and the mechanical cohesion is weakened as is illustrated in Fig. 1. Such "defects" in the glass structure can be treated by using the damage variable D of continuum damage mechanics (Kachanov [1], Lemaitre [2]). This parameter is proportional to the density of micro-defects. In preceding reports [5,6,7] we discussed the effect of water on the Young's modulus E, and showed that the water reaction reduces E, for small water concentrations proportional to the amount of water generated in the reaction.

The damage variable D can be interpreted as the part of the material cross-section that can no longer transmit forces. Consequently, the area that can carry load, A_D, is reduced to

$$A_D = A_0(1-D) \tag{2}$$

where A_0 denotes the total geometrical cross section subsuming damaged and undamaged regions.

According to the postulate of strain equivalence by Lemaitre [8], the effective elastic modulus, E_D, decreases with increasing damage

$$E_D = E_0(1-D) \tag{3}$$

where E_0 is the modulus of virgin glass.

The damage variable D can be determined from module measurements via eq.(3). To the authors' knowledge, so far no measurements on fused silica are available. Therefore, we temporarily consider the damage D as a certain function of the hydroxyl concentration:

$$D = f(S) \tag{4}$$

Apart from the equi-triaxial loading case with $\sigma_x = \sigma_y = \sigma_z$ (including the case of disappearing stresses), the elastic modulus must become a tensor with components depending on the degree of loading multiaxiality. Since this possibility would make the further treatment very difficult [8] and non-transparent, we assume in the following considerations that the damage remains isotropic and is considered to be of scalar nature. This is equivalent to the assumption of randomly orientated defects. Then also

E remains isotropic. We assume that nano-pores in SiO_2, caused by hydroxyl generation, might behave like normal pores.

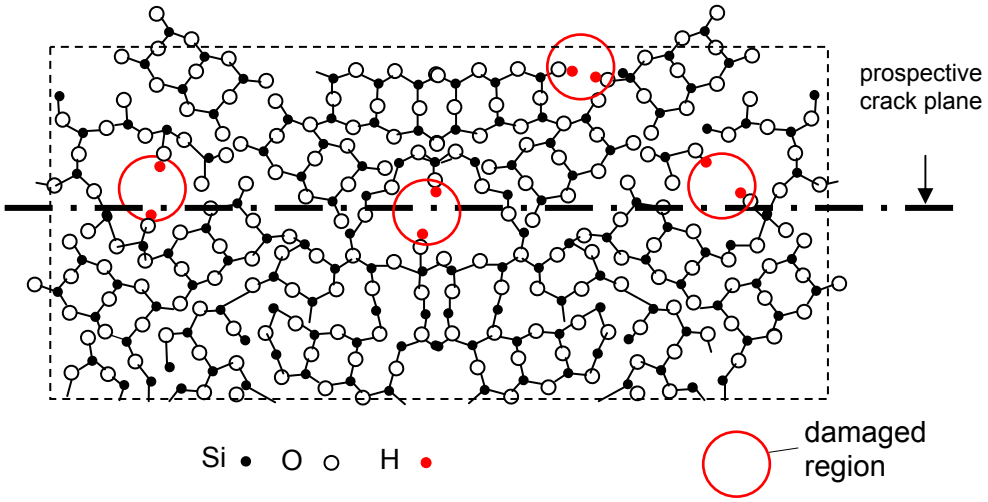

Fig. 1 Volume element of silica showing damage by bond breaking due to the water/silica reaction, third dimension ignored.

2 Experimental evidence for modulus reduction in silica

In literature, there is experimental evidence for modulus decrease with increasing hydroxyl content. This can be seen from measurements of Young's modulus as a function of water content. Measurements on longitudinal sound velocities and densities in silica specimens with different water content were reported by Fraser [9] and Le Parc et al. [10]. Individual least-squares fits were made resulting for the data set by Fraser [9]

$$v \cong 5974\,(1-4.185S) \quad \text{in (m/s)} \tag{5}$$

and the set by LeParc et al. [10]

$$v \cong 5959(1-5.34S) \quad \text{in (m/s)} \tag{6}$$

When we normalize the results of the two test series on their individual mean values for S=0, we get the representation in Fig. 2. A common straight-line fit of these data yields

$$\frac{v}{v_0} = 1 - B\,S \tag{7}$$

with the parameter

$$B=5.04\ [4.23,\ 5.85]$$

(90%-CI in brackets).

The dependency of eq. (7) is introduced in Fig. 2 as the straight line. Since the longitudinal sound velocity depends on Young's modulus E and density ρ via $v \propto \sqrt{E/\rho}$, (Poisson's ratio ν assumed to be constant) we obtain for small S:

$$\frac{E_D}{E_0} = \rho/\rho_0 \times (v/v_0)^2 = 1 - \lambda S \tag{8}$$

with λ=10.6 [8.7, 12.5]. It has to be noted that this value holds for isotropic damage since the natural OH-content doesn't show any preference for a special direction.

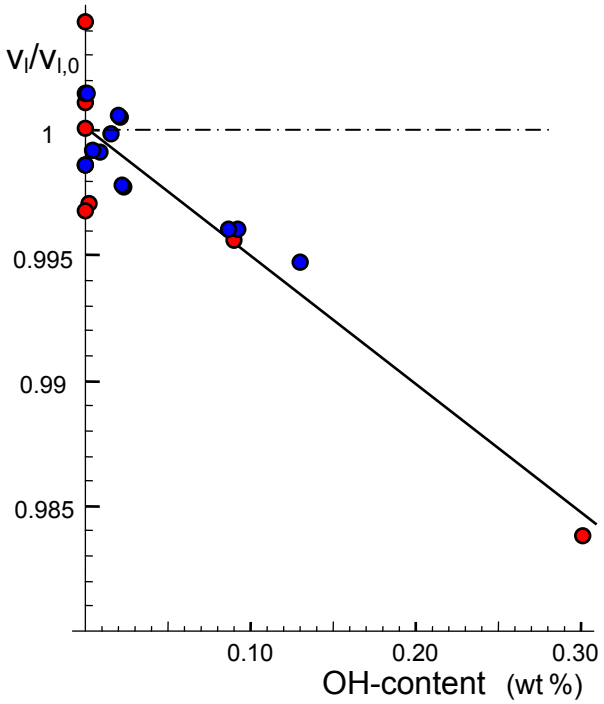

Fig. 2 Longitudinal sound velocity in silica with different OH-content (blue circles: results by Fraser [9], red circles: results by LeParc et al. [10]).

3 Modelling of damage by spherical pores

Analytical computations on the reduction of Young's modulus with porosity were carried out by Wang [3] for spherical pores. Unfortunately, the results were given as tabulated data. They were the basis of a number of fitting relations, mostly using exponential functions, which trivially must fail for large porosities since they could not represent the requirement of E=0 for a finite critical porosity. Wang [11] suggested a quadratic argument in the exponential function:

$$\frac{E_D}{E_0} = \exp[-A_1 P - A_2 P^2] \tag{9}$$

On the other hand, when P=1 (the whole volume is "pore") a finite modulus comes out what is of course not correct. An overview on descriptions can be obtained from [12, 13].

Wang [3] determined the effect of porosity on Young' modulus theoretically via model computations. He changed the porosity by compacting a cubic array of spheres with identical size. The analytical data were given in a Table for three cases: the ideal case 1 in which each particle center remains on the lattice symmetry lines; case 2 for shear effects included and case 3 for combined shear and hinge effects included. The results of the computations are shown in Fig. 3a by the circles. We described the numerically given data by Wang [3] for all the three cases by the equation

$$\frac{E_D}{E_0} = \exp\left[- A_1 P - \frac{A_2}{(P_{\max} - P)^{1/n}} P^2 \right] \tag{10}$$

with $P_{\max}$=0.4764 from [3]. The other parameters A_1, A_2, and n were obtained by curve fitting to the numerical data.

The results are compiled in Table 1. The fitting curves are entered in Fig. 3. In order to show the good agreement of the fitting equation with the numerical data, the confidence intervals are given for case 3. The very narrow 90% confidence intervals indicate the good agreement with the numerical data.

Case	A_1	A_2	n
1	1.0286	1.6699	6
2	2.3289	2.6190	7
3	3.580 [3.565, 3.595]	3.747 [3.699, 3.795]	8

Table 1 Fitting parameters for eq.(10)

Figure 3b shows the numerical solution by Wang [3] as the circles and the linear dependency for small porosities

$$\frac{E_D}{E_0} \cong 1 - A_1 P \tag{11}$$

as the dashed straight line that intersects the abscissa at a characteristic porosity P_c of

$$P_c = 1/A_1 = 0.278 P_{\max} \tag{12}$$

The description by eq.(10) is entered as the solid curve. Good agreement between eq.(10) and the numerical data can be stated over the full porosity range.

In order to give a better resolution for the agreement at low modules, Fig. 3c represents the same results in logarithmic ordinate scaling.

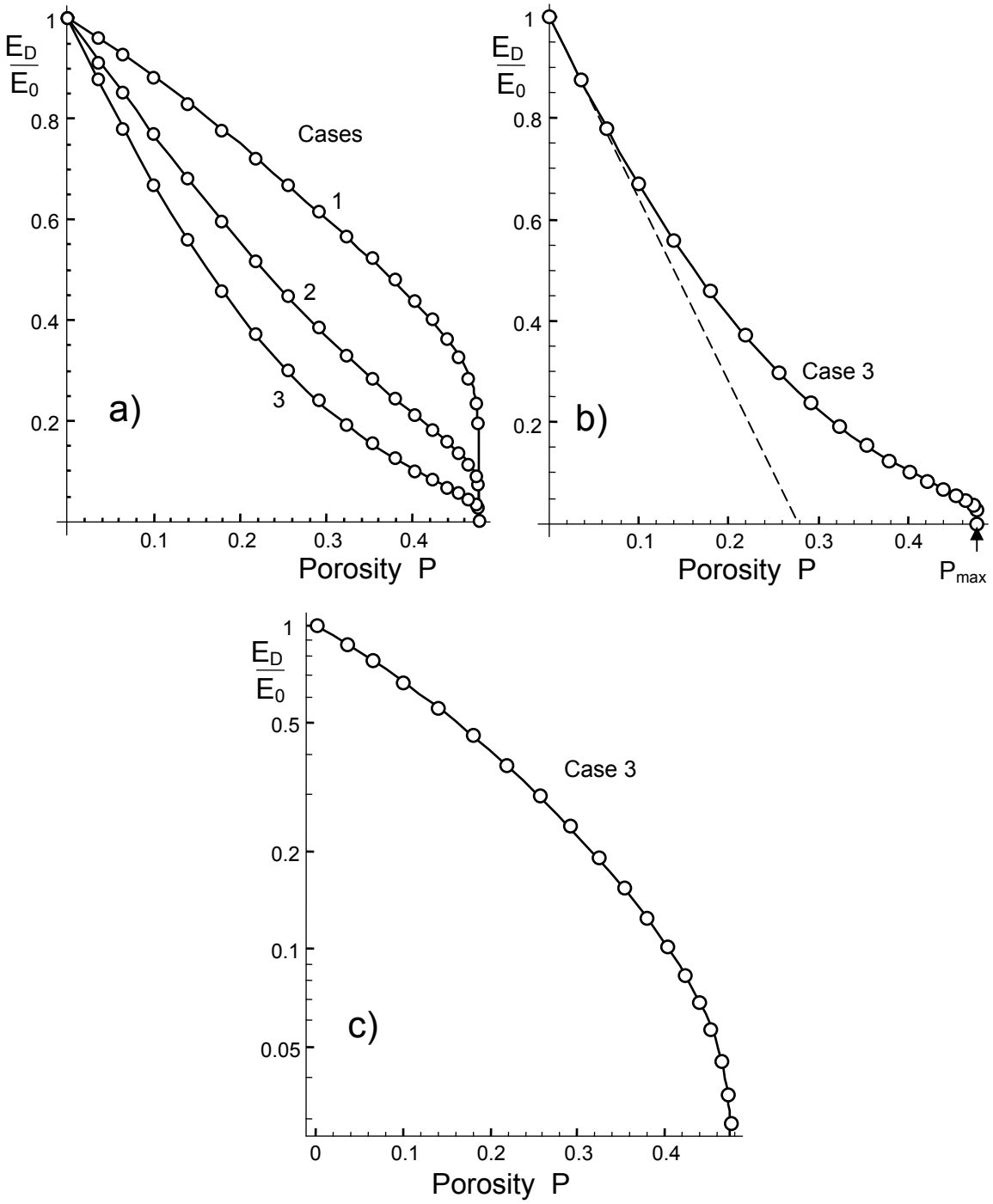

Fig. 3 Effect of porosity on Young's modulus for spherical pores; a) analytical results from Wang [3] (circles) compared with suggested fitting relation eq.(10) (curves); b) comparison of the approximation eq.(11) with eq.(10), c) logarithmic ordinate scaling of the data in Fig. 3b.

For our purpose we rewrite eq.(10) by normalizing the porosities on the maximum value P_{max} and then replace P by S

$$\frac{E_D}{E_0} = \exp\left[- B_1(S / S_{\max}) - \frac{B_2}{(1 - S / S_{\max})^{1/n}} \left(\frac{S}{S_{\max}} \right)^2 \right] \tag{13}$$

with the parameters n=8, B_1=1.667, B_2=0.933. The result is plotted in Fig. 4 together with the linear approximation. From eq.(8) and the initial slope of eq.(13) we obtain via $B_1/S_{\max}=\lambda$ the maximum value of hydroxyl concentration

$$S_{\max} = \frac{B_1}{\lambda} = 0.157 \;\; [0.133, 0.192] \tag{14}$$

A simpler pore model was proposed by Phany and Niyogi [4] with the simple result of

$$\frac{E_D}{E_0} = (1 - aP)^n \tag{15}$$

This type of equation applied to the hydroxyl damage gives good agreement with the Wang solution over a large range of hydroxyl concentrations for the parameter set

$$n = 2,\; a = \lambda/2 \cong 5.3 \tag{16}$$

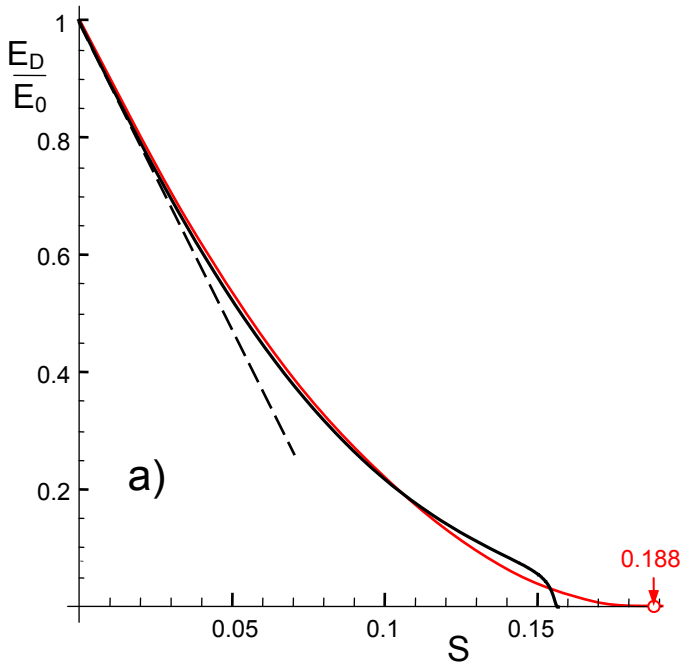

Fig. 4 Young's modulus as a function of hydroxyl concentration.

The related dependency is shown in Fig. 4 by the red curve that gives disappearing of Young's modulus at $S_{\max} = 0.188$ [0.16, 0.23]. The modulus ratio can be described by

$$\frac{E_D}{E_0} = (1 - \tfrac{1}{2}\lambda S)^2 \tag{17}$$

4 Application on crack-tip behaviour

At crack tips under externally applied loads, the singular stresses must result in high hydroxyl concentrations. This fact is known for instance in subcritical crack growth of glasses as can be concluded from the reaction rate theory and the molecular bond-splitting theory (for an overview see e.g. Freeman et al. [14]). Consequently, high damage has to be expected at crack tips followed by a strong stress reduction. As long as a positive crack-tip stress intensity factor exists, $K_{tip} \geq 0$, also stress singularity must exist with $\sigma_{ij} \rightarrow \infty$. The hydroxyl concentration must reach its maximum possible value, S_{max}, with the consequence that the damage must tend to $D \rightarrow 1$ and the Young's modulus must disappear at the tip, $E_D \rightarrow 0$. These consequences make the occurrence of singular stresses and a crack-tip stress intensity factor at least questionable.

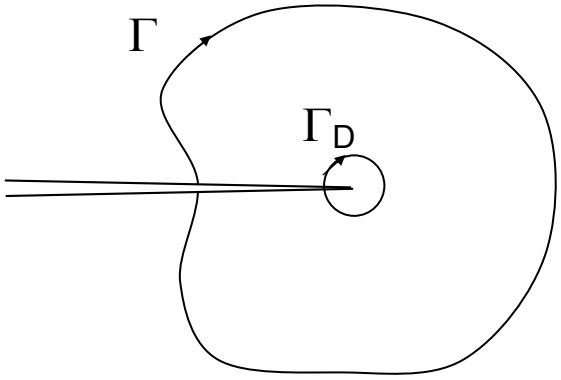

Fig. 5 Two J-integral paths around a crack tip; path Γ far away from the tip reflects the properties of the bulk material, path Γ_D the water-affected and damaged crack-tip region.

The problem will be discussed here by using the path-independence of the J-Integral by Rice [15]. For any time-independent material behaviour the fracture mechanics J-integral can be used as the loading parameter. It simply reads for linear-elastic materials

$$J = \frac{K^2(1-\nu^2)}{E} = G \tag{18}$$

where the right-hand side is also called the energy release rate G. Since the J-integral for any path around the crack tip is a parameter independent of the specially chosen path, its value must be the same for a path Γ far away from the tip (in the bulk) and the path Γ_D directly at the crack tip, i.e. in the damaged region as is illustrated in Fig. 5

$$\frac{K_{appl}^2(1-\nu_0^2)}{E_0} = \frac{K_{tip}^2(1-\nu_D^2)}{E_D} \tag{19a}$$

where E_D and ν_D are the elastic properties at the tip affected by water. For $\nu_D \cong \nu_0$

$$K_{tip} \cong K_{appl}\sqrt{\frac{E_D}{E_0}} \tag{19b}$$

This relation also holds for notches [16].

From eqs.(19b) and (17) a simple approximation for the crack-tip stress intensity factor is obtained:

$$K_{tip} \cong K_{appl}(1-\tfrac{1}{2}\lambda S) \tag{20}$$

Next, we will compute the local hydroxyl concentration and the damage as a function of the externally applied stress intensity factor K_{appl}.
At temperatures $T < 450°\text{C}$, the equilibrium constant k of the silica/water-reaction eq.(1) is

$$k = \frac{S}{C}. \tag{21}$$

Here C=[H_2O] is the concentration of molecular, and S=[SiOH] the concentration of hydroxyl water. The equilibrium constant for the reaction under pressure p is [17],[18]

$$\frac{\partial \ln k}{\partial p} = -\frac{\Delta \overline{V}}{RT}. \tag{22}$$

where p is pressure, $\Delta \overline{V}$ is the activation volume, R the universal gas constant and T the temperature in °K.
In applying eq.(22) to mechanical problems, it must be noted that the signing in mechanics differs from that in chemistry. In chemistry, pressures are regarded as <u>positive</u> variables, but are counted as <u>negative</u> stresses in continuum mechanics. This makes it necessary to replace the pressure p in eq.(22) by the hydrostatic stress term $-\sigma_h$, defined as the average of the three normal stress components of any stress tensor

$$\frac{\partial \ln k}{\partial \sigma_h} = \frac{\Delta \overline{V}}{RT} \tag{23}$$

The equivalent representation of eq. (23) is given by

$$\frac{k}{k_0} = \exp\left[\frac{\sigma_h \Delta \overline{V}}{RT}\right]. \tag{24}$$

where k_0 is the equilibrium constant in the absence of stresses. The hydrostatic stress under plane strain conditions is

$$\sigma_h(K_{tip}) = \tfrac{2}{3}(1+\nu)\frac{K_{tip}}{\sqrt{2\pi r}}\cos(\varphi/2) \tag{25}$$

where r and φ are polar coordinates with the origin at the crack tip. Crack extension under inert conditions occurs at fracture toughness K_{Ic}. Then the normal component σ_y on the prospective crack plane

$$\sigma_y = \frac{K_{\mathrm{Ic}}}{\sqrt{2\pi r}} \tag{26}$$

reaches a critical stress value σ_0. At the same location the hydrostatic stress ahead a crack tip, $\varphi=0$ is

$$\sigma_h = \tfrac{2}{3}(1+\nu)\,\frac{K_{tip}}{K_{Ic}}\sigma_0 \tag{27}$$

The fracture toughness of silica is $K_{\mathrm{Ic}} = 0.8$ MPa$\sqrt{\mathrm{m}}$ [19] and the theoretical strength is about [20]

$$\sigma_0 = \frac{E}{\pi} \cong 23\,\mathrm{GPa} \tag{28}$$

as is in agreement with strengths up to 25GPa measured by Brambilla and Payne [21] on extremely thin silica fibers of about 60 nm radius. The highest tensile strengths for thicker silica glass fibers in ultra high vacuum at room temperature are about $\sigma_c \cong$ 12.6 GPa [22].

From eqs.(24) and (27) it follows

$$S = S_0 \exp\left[\lambda \frac{K_{tip}}{K_{\mathrm{Ic}}}\right], \quad \gamma = \tfrac{2}{3}(1+\nu)\frac{\sigma_0 \Delta\overline{V}}{RT} \tag{29}$$

and with the approximate solution, eq.(20),

$$S = S_0 \exp\left[\gamma \frac{K_{appl}}{K_{\mathrm{Ic}}}(1 - \tfrac{1}{2}\lambda\, S)\right] \tag{30}$$

The unknown quantity S appears on both sides of eq.(30). This implicit equation in S is solved by

$$S = S_{\max}\frac{K_{\mathrm{Ic}}}{\gamma K_{appl}}\,\mathrm{PLog}\left[\gamma \frac{K_{appl}}{S_{\max}K_{\mathrm{Ic}}} S_0 \exp\left(\gamma \frac{K_{appl}}{K_{\mathrm{Ic}}}\right)\right] \tag{31}$$

where the "PLog" stands for the Lambert W function or *product log function*, i.e. the solution $W=\mathrm{PLog}(z)$ of the equation $z = W\exp(W)$ [23].

Due to eq.(20) a similar relation holds for the crack-tip stress intensity factor

$$K_{tip} = K_{appl}\left(1 - \frac{K_{\mathrm{Ic}}}{\gamma K_{appl}}\,\mathrm{PLog}\left[\gamma \frac{K_{appl}}{S_{\max} K_{\mathrm{Ic}}} S_0 \exp\left(\gamma \frac{K_{appl}}{K_{\mathrm{Ic}}}\right)\right]\right) \tag{32}$$

The solutions for S and K_{tip} are shown in Fig. 6 in normalized representation. The hydroxyl concentration in the absence of stresses, S_0, results from the total water concentration by Zouine et al. [24] and the equilibrium constant $k_0 \cong 0.41$ according to [25]. At room temperature we obtain $S_0 \cong 0.035$ wt%.

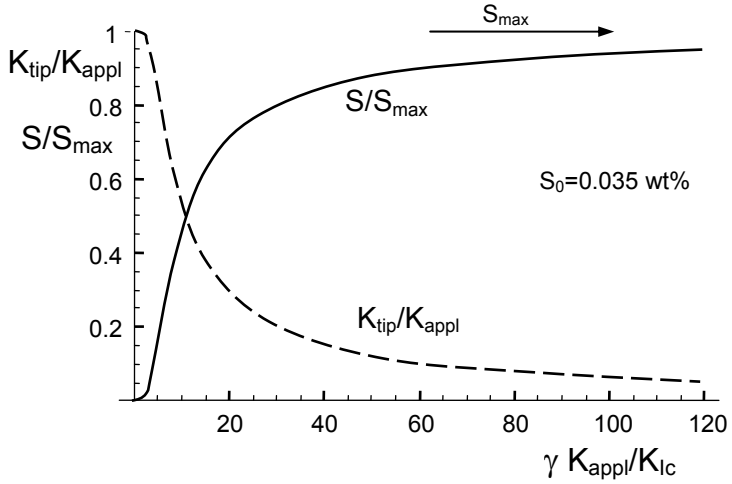

Fig. 6 Hydroxyl concentration S and crack-tip stress intensity factor K_{tip} as a function of $\gamma \times K_{\mathrm{appl}}/K_{\mathrm{Ic}}$ for $S_0 \cong 0.035$ wt% as obtained for room temperature.

5 Examples of application

5.1 Crack-tip stress intensity factor and hydrostatic stress

For an example let us use $\Delta\overline{V} = 15\ \mathrm{cm}^3/\mathrm{mol}$, $\nu = 0.17$, $K_{\mathrm{Ic}} = 0.8\ \mathrm{MPa}\sqrt{\mathrm{m}}$. At room temperature, a typical stress intensity factor in subcritical crack growth experiments is $K_{\mathrm{appl}} = 0.4\ \mathrm{MPa}\sqrt{\mathrm{m}}$.

Then we obtain on the basis of eq.(17):

S=16.7 wt%, $E \cong 0.95$ GPa, $K_{\mathrm{tip}} \cong 0.045\ \mathrm{MPa}\sqrt{\mathrm{m}}$, σ_h =1.01 GPa for σ_0=23 GPa

S=15.2 wt%, $E \cong 2.7$ GPa, $K_{\mathrm{tip}} \cong 0.078\ \mathrm{MPa}\sqrt{\mathrm{m}}$, σ_h =0.99 GPa for σ_0=13 GPa

The corresponding results obtained by numerical evaluation of eq.(12) are

$S \cong 15.7$ wt%, $E \cong 0.88$ GPa, $K_{\mathrm{tip}} \cong 0.044\ \mathrm{MPa}\sqrt{\mathrm{m}}$, σ_h =0.993 GPa for σ_0=23 GPa

S=15.5 wt%, $E \cong 2.76$ GPa, $K_{\mathrm{tip}} \cong 0.078\ \mathrm{MPa}\sqrt{\mathrm{m}}$, σ_h =0.991 GPa for σ_0=13 GPa

From these examples it becomes obvious that the Young's modulus and the crack-tip stress intensity factor are drastically reduced for cracks loaded in water.

The solutions for K_{tip} and σ_h are shown in Fig. 7a in dependence of the applied stress intensity factor for strongly varied hydroxyl concentration in the absence of stresses, S_0.

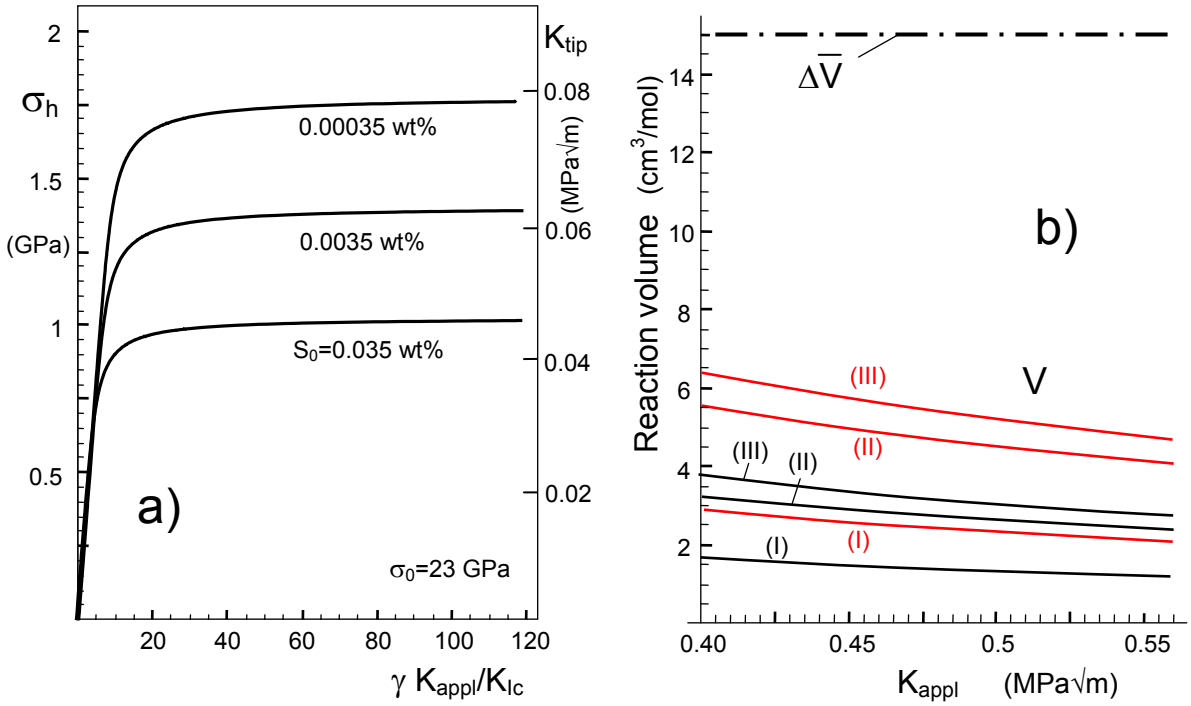

Fig. 7 a) Hydrostatic stress σ_h and crack-tip stress intensity factor K_{tip} as a function of the applied stress intensity factor K_{appl}, b) apparent reaction volume for subcritical crack growth (black curves: σ_0=23 GPa, red curves: σ_0=13 GPa), (I) mathematically sharp crack, (II) plain strain conditions and (III) plane stress conditions at a slender notch.

5.2 Apparent reaction volume

In the case of subcritical crack growth experiments, the *v-K* curves are plotted usually against the *applied* stress intensity factor K_{appl} and not versus the crack-tip stress intensity factor K_{tip}. Therefore, the product $K_{tip}\Delta\overline{V}$ used in reaction rate theory may be replaced by the measurable K_{appl} combined with an apparent reaction volume V resulting in the same value, namely

$$K_{tip}\Delta\overline{V} = K_{appl}V \tag{33}$$

Since $K_{appl} > K_{tip}$, it must hold $V < \Delta\overline{V}$. The apparent reaction volume is plotted in Fig. 7b for different crack models and different strengths σ_0. The red curves show results for $\sigma_0 = 13$ GPa, the black curves for $\sigma_0 = 23$ GPa. The curves indicated by (I) were computed with the apparent volume for the hydrostatic stresses ahead the tip of a sharp crack according to eq.(27). Sometimes, the crack-tip region is modeled by a slender notch with a finite notch root in the order of the "micro-structure", i.e. the silica ring

structure. A notch-root radius of 0.5 nm was for instance suggested by Wiederhorn et al. [26]. Under *plain strain* conditions it holds at a notch root

$$\sigma_h = \tfrac{1}{3}(1+\nu)\,\frac{K_{tip}}{K_{Ic}}\sigma_0 \tag{34}$$

and under *plane stress* conditions

$$\sigma_h = \tfrac{1}{3}\,\frac{K_{tip}}{K_{Ic}}\sigma_0 \tag{35}$$

Equation (34) results in the curves indicated by (II) and in case of eq.(35) the curves are marked as (III). In all cases the apparent reaction volume is clearly smaller than the true reaction volume of $\Delta\overline{V}$ =15 cm^3/mol introduced by the dash-dotted line in Fig. 7b.

Summary

We studied the effect of hydroxyl generation accompanied by damaging the initial SiO_2 ring structure. For the mathematical treatment, the damage variable *D* was used that describes the effective reduction of the load-carrying cross section as suggested by Lemaitre [2]. Results from literature on sound velocity by Fraser [9] and Le Parc et al. [10] were transformed into a relation between the Young's modulus for the damaged glass and the hydroxyl concentration. As an application of the relation between hydroxyl concentration, damage, and Young's modulus, we estimated the effect of these parameters at mechanically loaded crack tips. Strong reduction of crack-tip stress intensity factor and Young's modulus are visible.

References

1 L.M. Kachanov, Time of the rupture process under creep conditions, TVZ Akad Nauk S.S.R. Otd Tech. Nauk **8**(1958).

2 J. Lemaitre, Evaluation of dissipation and damage in metals, Proc. I.C.M. 1, Kyoto Japan (1971).

3 J.C. Wang, Young's modulus of porous materials, Part 1, J. Mater. Sci. **19**(1984), 801-808.

4 Phani, K.H. Niyogi, K. De, Young's modulus of porous brittle solids, J. Mater. Sci. **22**(1987), 257–263.

5 T. Fett, G. Schell, Consequence of Damage in Silica on Young's Modulus, Scientific Working Papers **51**, 2018, ISSN: 2194-1629, Karlsruhe, KIT.

6 T. Fett, G. Schell, Damage in silica by hydroxyl generation described by Wang's theoretical data, Scientific Working Papers **85**, 2018, ISSN: 2194-1629, Karlsruhe, KIT.

7 T. Fett, G. Schell, Damage in silica by hydroxyl generation: Behaviour at crack tips Scientific Working Papers **87**, 2018, ISSN: 2194-1629, Karlsruhe, KIT.

8 J. Lemaitre, How to use damage mechanics, Nuclear Engng. Design **80**(1984), 233-245.

9 D.B. Fraser, Factors Influencing the Acoustic Properties of Vitreous Silica, Citation: Journal of Applied Physics 39(1968), 5868-5878.

10 R. Le Parc, C. Levelut, J. Pelous, V. Martinez, B. Champagnon, Influence of fictive temperature and composition of silica glass on anomalous elastic behavior *J. Phys.: Condens.* Matter **18**(2006), 7507-27.

11 Wang, J.C., Young's modulus of porous materials, Part 2, *J Mater Sci*. 1984;19:809-814.

12 Phani, K.H., Niyogi, S.K., Elastic-modulus–porosity relationship for Si_3N_4, J. Mater. Sci. Letters **6**(1987), 511–515.

13 Phani, K.H. Niyogi, K. De, Porosity dependence of fracture mechanical properties of reaction sintered Si_3N_4, J. Mater. Sci. Letters **7**(1988), 1253–1256.

14 Freiman, S.W., Wiederhorn, S.M., Mecholsky, J.J., J. Am. Ceram. Soc. **92**(2009), 1371-1382.

15 Rice, J.R., A path independent integral and the approximate analysis of strain concentration by notches and cracks, Trans. ASME, J. Appl. Mech. (1986), 379-386.

16 J. G. Merkle, An application of the J-integral to an incremental analysis of blunt crack behavior, Mechanical Engineering. Publications, London, 1991, 319-332.

17 Le Chatelier H, *CR Acad Sci Paris.* 99;1884:786.

18 Hamann SD. *High Pressure Physics and Chemistry*, Ed. Bradley RS. Academic Press, London. 1963:163-207.

19 S.M. Wiederhorn, Fracture surface energy of glass, J. Am. Ceram. Soc. **52** (1969), 99-105.

20 Silva, E. C. C. M.; Tong, L.; Yip, S.; Van Vliet, K. J. *Small* **2005**, *2*, 239–243.

21 G. Brambilla, D.N. Payne, The ultimate strength of glass silica nanowires, Nano Letters, **9**(2009), 831-835.

22 C.R. Kurkjian, P.K. Gupta, R.K. Brow, and N. Lower, "The intrinsic strength and fatigue of oxide glasses," *J. Noncrystal. Solids*, **316** 114-124 (2003).

23 R. Corless, G. Gonnet, D. Hare, D. Jeffrey and D. Knuth, "On the Lambert W Function," Advances in Computational Mathematics, **5**(1996), 329-359.

24 A. Zouine, O. Dersch, G. Walter and F. Rauch, "Diffusivity and solubility of water in silica glass in the temperature range 23-200°C," *Phys. Chem. Glass: Eur. J. Glass Sci and Tech. Pt. B*, **48** [2] 85-91 (2007).

25 S. M. Wiederhorn, F. Yi, D. LaVan, T. Fett, M.J. Hoffmann, Volume Expansion caused by Water Penetration into Silica Glass, J. Am. Ceram. Soc. **98** (2015), 78-87.

26 S.M. Wiederhorn, E.R. Fuller, Jr. and R. Thomson, "Micromechanisms of crack growth in ceramics and glasses in corrosive environments," Metal Science, **14**(1980), 450-8.

KIT Scientific Working Papers
ISSN 2194-1629

www.kit.edu